ASTRONOMY & ASTROPHYSICS
SUPPLEMENT SERIES

Astron. Astrophys. Suppl. Ser. **119,** 547-557 (1996)

Infrared aperture photometry at ESO (1983–1994) and its future use⋆,⋆⋆

N.S. van der Bliek[1,2,⋆⋆⋆], J. Manfroid[3,†] and P. Bouchet[1]

[1] European Southern Observatory, Casilla 19001, Santiago 19, Chile
[2] Sterrewacht Leiden, Postbus 9513, 2300RA Leiden, The Netherlands
[3] Departement d'Astrophysique de l'Université de Liège, Avenue de Cointe 5, B-4000 Liège, Belgium

Received March 8; accepted March 15, 1996

Abstract. — We describe the infrared (IR) photometric system for the single channel photometers at ESO, which have been used from 1983 until 1994. In addition to the broadband near infrared (NIR, 1−5 μm) photometric system presented in 1991 by Bouchet et al. and Bersanelli et al., we describe a *narrow*-band NIR photometric system and a *mid* infrared (MIR, 7−20 μm) photometric system. We also extend the set of NIR standard stars by Bouchet et al. towards fainter objects ($K \simeq 9$). The photometric data of the standard stars in these systems were extracted from the complete IR photometric data archive of ESO, covering 10 years. The zeropoints of the NIR photometry are set by assuming that HR 3314 has a V-magnitude of 3.89, and that $V-K=-0.05$, $J-K=-0.01$, $H-K=-0.01$, $K-L'=0.00$, $K-M=0.00$. The zeropoints of the MIR photometry are set by assuming that the colours of β Hyi (HR 0098) and α CenA (HR 5459) are equal to the colours of the Sun. We adopt the absolute calibration of Mégessier (1995) for the NIR and we argue that this calibration can be extrapolated to 20 μm, using the MIR calibrations by Rieke et al. (1985) and Cohen et al. (1992). The definition of the zeropoints is consistent with the absolute calibration. We obtained accurate ($\sigma \simeq 0.02$ mag.) NIR photometry of about 240 standard stars and MIR photometry of about 40 standard stars ($\sigma \simeq 0.04$ mag). Comparison of our NIR photometric system with other well established systems shows that there are some small colour dependencies and zeropoint offsets which are always smaller than about 0.02 mag. except for the L' band.

Key words: instrumentation: photometers — techniques: photometric — infrared: stars

1. Introduction

Recent developments in infrared (IR) astronomy allow us to observe fainter sources, to obtain more accurate data and even to observe at previously unexploited wavelengths. For example, with near-infrared (NIR) and 10 μm arrays, one can observe several magnitudes deeper than with the single channel detectors. With the instruments of the Infrared Space Observatory (ISO) observations can be made out to 200 μm. In addition, IR astronomy has also come to the stage that spectrophotometry is feasible. These new observations require an extension of the available calibration sources or even a completely new set of calibration sources and for spectrophotometric applications energy distributions of calibration stars should replace the photometric data.

When extending an existing or newly defining a set of standard stars, the first step is to analyse all data that are already available. In this paper we analyse the complete IR photometric archive of ESO and present the ESO IR photometric system for the single channel photometers. These photometers were used from 1983 to 1994 at the ESO 3.6 m, the ESO/MPI 2.2 m and the ESO 1 m telescopes. They have been taken out of service. The system we describe includes the ESO broadband NIR and *mid* infrared (MIR) filters and a set of *narrow*-band NIR filters, which are narrow passbands corresponding to specific positions of two NIR circular variable filters (CVFs). In 1991 Bouchet et al. (hereafter BMS91) and Bersanelli et al. described the ESO NIR *broad*-band system. We extend their work in the NIR towards fainter objects ($K \simeq 9$). We add the NIR *narrow*-band system and we describe the MIR photometric system.

Send offprint requests to: N.S. van der Bliek
⋆based on observations made at the European Southern Observatory, La Silla, Chile
⋆⋆Tables 5-7 are only available in electronic form at the CDS via anonymous ftp 130.79.128.5
⋆⋆⋆*Present address:* Sterrewacht Leiden, Postbus 9513, 2300RA Leiden, The Netherlands
†Research director, Belgian national fund for scientific research (FNRS)

The paper is arranged as follows. In Sect. 2 we describe the properties of the passbands used. In Sect. 3 we define the zeropoints of the magnitude scales and we present our absolute calibration. The observational data base is described in Sect. 4 and the data reduction method in Sect. 5. In Sect. 6 we present the photometric data on the calibration stars. In Sect. 7 we finish with some concluding remarks.

2. Description of the passbands

The ESO IR photometers are single channel photometers with an InSb detector for the NIR and a bolometer for the MIR (Bouchet 1989). The InSb photometers are equipped with seven broadband filters and three CVFs: 1.5−2.5 μm, 2.5−4.5 μm and 4.1−5.5 μm ($\lambda/\Delta\lambda \simeq 70$). The bolometer photometers were equipped with ten broadband filters and one CVF: 8−14 μm. The IR system we describe in this paper is the most commonly used subset and consists of

- an InSb detector and 5 broadband NIR filters: J, H, K, L' and M;
- an InSb detector and 5 (narrow) passbands within two NIR CVFs centered around: 1.58 μm (H_0), 2.16 μm ($Br\gamma$), 2.22 μm (K_0), 2.29 μm (CO) and 3.70 μm (L_0);
- a bolometer and 5 broadband MIR filters: N, N_1, N_2, N_3 and Q_0.

The narrowband filters were defined for the project 'Infrared Standard Stars for ISO' (see e.g. van der Bliek et al. 1992), where narrowband photometry is used to determine stellar temperatures with the Infra-Red Flux Method by Blackwell et al. (1980). For narrowband photometry no colour corrections depending on the spectral energy distribution need to be applied and narrowband measurements are less affected by the colour dependence of the atmospheric extinction than broadband measurements. For IR photometry it is particularly important to use narrowband filters, with passbands not determined by the atmospheric absorption (see also the recommendations made by Young et al. 1993, 1994).

Filter transmission curves, including detector responses, are displayed in Figs. 1-4. Although there were four frequently used InSb detectors and three bolometers, we only display one transmission curve. The systems are rather homogeneous, because the filters were cut from the same material and the detectors are near identical. We found that the transmission curves of the different detector-filter combinations were identical to within 1%. The transmission curves were measured under the same cryogenic conditions as when the detectors were operational at the telescope.

In the figures the transmission of the Earth's atmosphere is also shown. Since no atmospheric transmission curve for La Silla exists, we have constructed one as follows: i) We used UKIRT atmospheric transmission curve for 1.2 mm H_2O, sec $z = 1.00$ and with a resolving power of about 3000 (Aspin 1995); ii) We have assumed that the Kitt Peak transmission curves by Manduca & Bell (1979), ranging from 1 to 2.6 μm, are a good approximation for the transmission at La Silla. This is a reasonable assumption as La Silla observatory and Kitt Peak observatory have about the same altitude; iii) We scale the UKIRT curve to the average of the Kitt Peak winter and summer curve and we assume that this scaling is also valid for longer wavelengths. We found that a transmission curve for which the absorption features were twice as deep as in the UKIRT transmission, gave the best representation of the average Kitt Peak curve. Note that the scaled atmospheric transmission is only an approximation of the La Silla transmission curve. When increasing the optical depth, the shape of the absorption features also changes. In Figs. 1-4 the scaled atmospheric transmission curve is shown.

In Table 1 effective wavelengths of the filters are given, together with the fullwidth halfmaxima (FWHM) of the filters. The effective wavelength $\lambda_{\rm eff}$, also called mean wavelength, is defined as follows

$$\lambda_{\rm eff} = \frac{\int \lambda\ S(\lambda)\ A(\lambda)\ {\rm d}\lambda}{\int S(\lambda)\ A(\lambda)\ {\rm d}\lambda} \qquad (1)$$

where $S(\lambda)$ is the sensitivity of the instrumental system, i.e. the filter transmission plus the detector response and $A(\lambda)$ the atmospheric transmission. This definition is chosen because instrumental magnitudes behave to a first-order approximation like monochromatic magnitudes at a wavelength $\lambda_{\rm eff}$ (cf. e.g. King 1952). In Kings original definition only the sensitivity of the instrumental system is taken into account, but this is not sufficient for the case of groundbased IR photometry. Most IR passbands, especially the broader ones, are much affected by the transmission of the Earth's atmosphere, and sometimes the cut-on and/or cut-off wavelengths are effectively determined by the atmospheric transmission. We have therefore included the atmospheric transmission in our definition of $\lambda_{\rm eff}$. Differences in $\lambda_{\rm eff}$ calculated with or without the atmospheric transmission can be several percent. For example $\lambda_{\rm eff}$ of the J band is 1.264 μm when taking into account only the instrumental sensitivity, but when including the atmospheric transmission $\lambda_{\rm eff}$ shifts to 1.228 μm. Note that the effective wavelengths defined in this way are not determined uniquely, because atmospheric conditions vary.

However, when converting observed magnitudes into absolute fluxes, one is interested in wavelengths representing the instrumental and atmospheric sensitivity times the observed spectrum, rather than in the effective wavelength of Eq. (1). In other words, to correctly convert magnitudes into fluxes, an assumption regarding the observed spectrum is necessary. In Table 1 we have added a column with such 'true' effective wavelengths for stellar spectra, $F(\lambda)$, assuming $F(\lambda)$ to be a black body of 11400 K:

$$\lambda_{\rm eff,\ 'true'} = \frac{\int \lambda\ F(\lambda)\ S(\lambda)\ A(\lambda)\ {\rm d}\lambda}{\int F(\lambda)\ S(\lambda)\ A(\lambda)\ {\rm d}\lambda} \qquad (2)$$

A black body of 11400 K is chosen, because this black body is used for the absolute calibration (see Sect. 3). The choice of this black body results in 'true' effective wavelengths which are reasonable for a wide range of stellar temperatures. A black body of 4000 K for example, shifts the $\lambda_{\rm eff}$ of the J band by 0.6%, and less for the other bands.

Uncertainties in the $\lambda_{\rm eff}$'s due to variations in the atmospheric transmission, are of the order of 0.005 μm in the NIR and 0.05 μm in the MIR. The $\lambda_{\rm eff}$'s of the narrowband filters are not affected by the atmospheric transmission. These uncertainties were determined by varying the scaling factor to convert the UKIRT atmospheric transmission curve into a La Silla transmission curve from 1.5 to 2.5.

The FWHMs of the filter passbands given in Table 1 are determined by folding the filter transmission with both the detector response and the atmospheric transmission. Variations in FWHM due to changes in the atmospheric transmission are of the order of 5 to 10% for most of the broadband filters. The FWHM of the H and K filter are much less sensitive to variations in the atmospheric transmission; they vary by at most 1%. The Q_0 filter is much more affected by atmospheric variations and has an uncertainty of about 15%. The FWHM of the narrowband filters are almost unaffected by variations in the atmospheric transmission: they vary by less than 1%.

3. The zeropoints of the magnitude scale and the absolute calibration

There are various ways to define the zeropoints of the magnitude scale of a photometric system. The most straightforward way is to define the magnitudes of a single star, the primary standard star. For the northern hemisphere Vega (HR 7001, α Lyr) is often used as primary standard (Elias et al. 1982). For the southern hemisphere Jones & Hyland (1982) and Allen & Cragg (1983) use HR 3314 as primary standard. Both Vega and HR 3314 are A0V stars. Another approach is to define the zeropoints such that the colours of an average A0 star are zero (e.g. Johnson 1965). This method has been used by Carter (1990) and McGregor (1994). We have chosen to define the magnitude scale of the ESO photometric system using one primary standard star. This is a transparent definition, and given the logic in the data reduction package used it is also the most convenient choice.

Once the magnitude scale is defined, an absolute calibration of this scale can be determined by measuring the fluxes of standard stars. However, if one is not in the position to actually measure the fluxes of the standard stars, one has to adopt an absolute calibration from the literature. The zeropoints of the magnitude scale have then

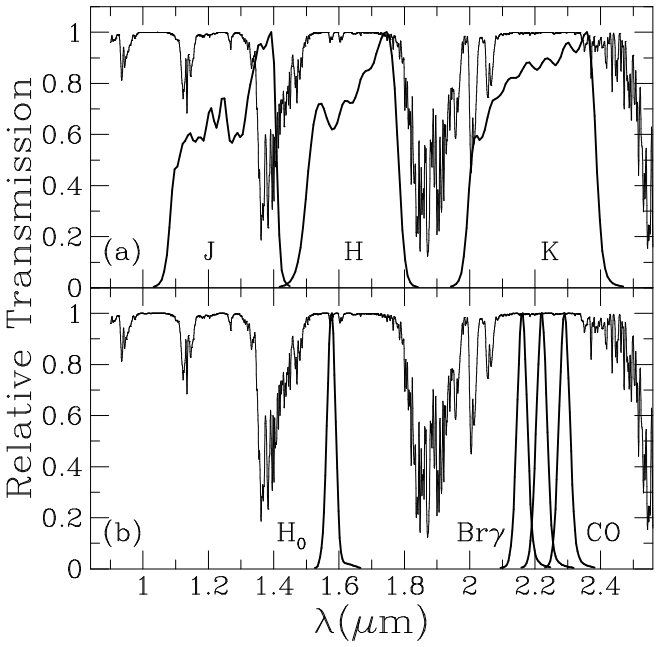

Fig. 1. Filter transmission times detector response in the 1−2.5 μm range (broad line) and the Earth's atmospheric transmission (thin line). **a)** The ESO broadband J, H and K filters; **b)** The ESO narrow band H_0; $Br\gamma$, K_0 and CO filters

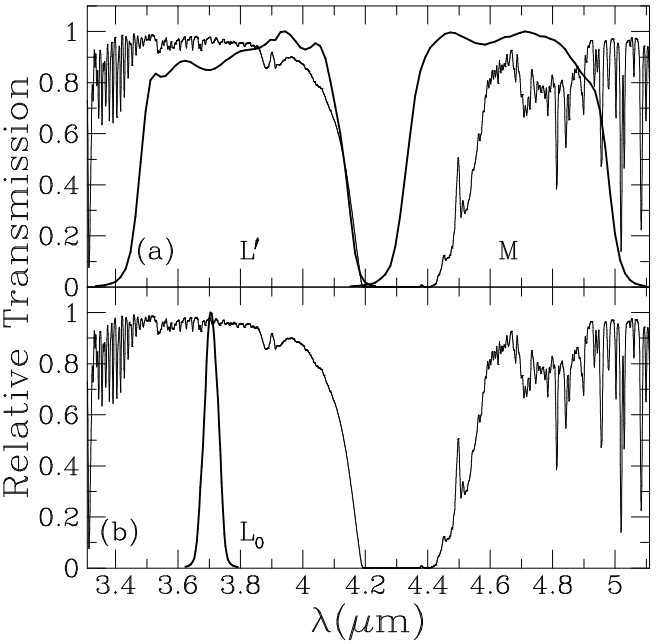

Fig. 2. Filter transmission times detector response in the 3−5.5 μm range (broad line) and the Earth's atmospheric transmission (thin line). **a)** The ESO broadband L' and M filters; **b)** The ESO narrowband L_0 filter

Table 1. Effective wavelengths, $\lambda_{\rm eff}$ (μm), fullwidth halfmaxima, FWHM (μm), and zero-magnitude fluxes for the ESO IR photometric passbands. The effective wavelengths are given following both definitions described by Eqs. (1) and (2). The zero-magnitude fluxes are calculated following Mégessier (1995) for the 'true' $\lambda_{\rm eff}$'s of Eq. (2)

filter	$\lambda_{\rm eff}$ (1) (μm)	$\lambda_{\rm eff,\ 'true'}$ (2) (μm)	FWHM (μm)	$F_{\lambda,(2)}(m_\lambda = 0)$ (W m^{-2} nm^{-1})	$F_{\nu,(2)}(m_\lambda = 0)$ (Jy)
J	1.228	1.210	0.190	3.44 10^{-12}	1.68 10^{3}
H	1.651	1.635	0.269	1.21 10^{-12}	1.07 10^{3}
K	2.216	2.197	0.360	4.12 10^{-13}	6.64 10^{2}
L'	3.771	3.740	0.580	5.58 10^{-14}	2.60 10^{2}
M	4.772	4.759	0.381	2.21 10^{-14}	1.67 10^{2}
H_0	1.577	1.577	0.031	1.37 10^{-12}	1.14 10^{3}
$Br\gamma$	2.161	2.161	0.037	4.38 10^{-13}	6.83 10^{2}
K_0	2.221	2.220	0.038	3.97 10^{-13}	6.53 10^{2}
CO	2.291	2.290	0.039	3.54 10^{-13}	6.19 10^{2}
L_0	3.706	3.706	0.050	5.78 10^{-14}	2.65 10^{2}
N	11.055	9.862	5.47	1.29 10^{-15}	4.17 10^{1}
N_1	8.361	8.328	0.72	2.50 10^{-15}	5.78 10^{1}
N_2	9.787	9.650	1.57	1.40 10^{-15}	4.35 10^{1}
N_3	12.819	12.774	1.15	4.64 10^{-16}	2.53 10^{1}
Q_0	18.666	18.425	3.23	1.09 10^{-16}	1.23 10^{1}

to be matched to this absolute calibration, instead of the other way around.

We have not measured absolute fluxes of any of our standard stars and thus we have to match the zeropoints of our magnitude scale to an absolute calibration. We adopt the absolute flux calibration of Mégessier (1995, hereafter M95). Based on a re-analysis of the absolute calibration of Vega at 5556 Å, M95 improves the NIR calibration of Bersanelli et al. (1991). She finds that a black body with a temperature of 11400 K, normalised to a zero-magnitude flux at 5556 Å of 3.56 10^{-11} Wm^{-2}nm^{-1}, gives the best fit to the collection of NIR absolute calibrations considered.

3.1. *The NIR photometry*

For the definition of the zeropoints of the NIR photometry, we use HR 3314. We assume that the V magnitude of HR 3314 is 3.89 (Rufener 1988) and we set the colours of HR 3314 to $V-K$=−0.05, $J-K$=−0.01, $H-K$=−0.01, $K-L'$=0.00 and $K-M$=0.00. These colours are dictated by the fact that M95 bases the absolute calibration on $J_{\rm Vega}$=$H_{\rm Vega}$=$K_{\rm Vega}$=+0.02 and that $J_{\rm HR\ 3314} - J_{\rm Vega}$ = 3.913, $H_{\rm HR\ 3314} - H_{\rm Vega}$ = 3.914 and $K_{\rm HR\ 3314} - K_{\rm Vega}$ = 3.919 (Elias et al. 1982, 1983). We have no information on $L'_{\rm HR\ 3314} - L'_{\rm Vega}$ and $M_{\rm HR\ 3314} - M_{\rm Vega}$, but we do know that the colours of HR 3314 should be zero or almost zero, because it is an A0V star. We have therefore set $(K-L')_{\rm HR\ 3314}$=0.00 and $(K-M)_{\rm HR\ 3314}$=0.00.

We tie the zeropoints of the narrowband photometry to the broadband photometry of HR 3314: H_0=H, $Br\gamma$=K_0=CO=K and L_0=L'. Note that the H_0 and $Br\gamma$ filters cover lines from the Bracket series, which are in absorption in the spectra of A-type stars (Fig. 5). One could therefore argue that the zeropoint should be defined such that the continuum flux of the spectrum of a zero-magnitude A0V star corresponds to magnitude zero. We have however chosen to stick to the definition that the colours of the A-type stars are near-zero and we compensate in the absolute calibration for the presence of absorption lines.

The zero-magnitude fluxes are given in Table 1. The zero-magnitude fluxes for the broadband NIR photometry are the black body fluxes corresponding to the effective wavelengths of Eq. (2), the 'true' effective wavelengths for stellar spectra. We decreased the zero-magnitude fluxes of the H_0 and $Br\gamma$ band by 1 and 2.5%, respectively, on the basis of the medium resolution spectrum of HR 2421, an A0IV star.

3.2. *The MIR photometry*

Because we do not have MIR data for HR 3314, we establish the zeropoints under the assumption that the two solar analogues in our sample, β Hyi (HR 0098) and α CenA (HR 5459) (Hardorp 1978; Hardorp 1982), have solar colours (cf. Thomas et al. 1973). We calculate the solar colours by folding the solar irradiance spectrum by Labs & Neckel (1970) with the Geneva V band (Rufener & Nicolet 1988) and with the ESO bands. However, before we can

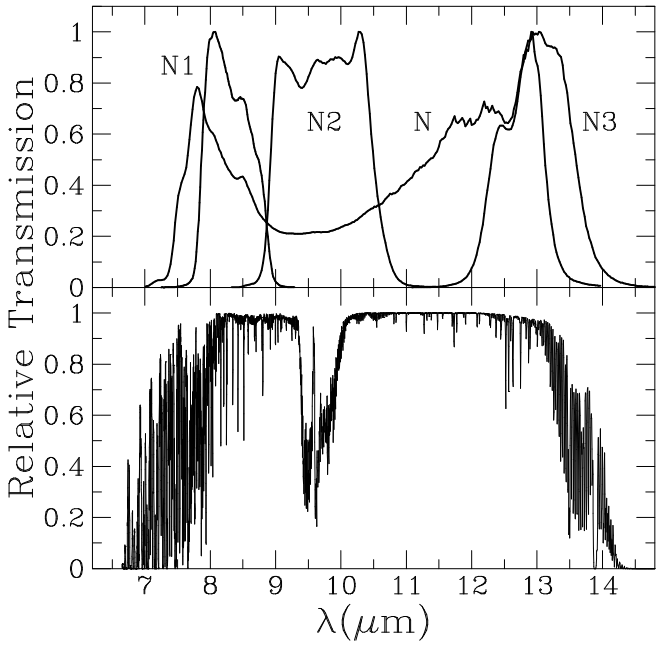

Fig. 3. Filter transmission times detector response at 10 μm, N, N_1, N_2 and N_3 (top) and the Earth's atmospheric transmission (bottom)

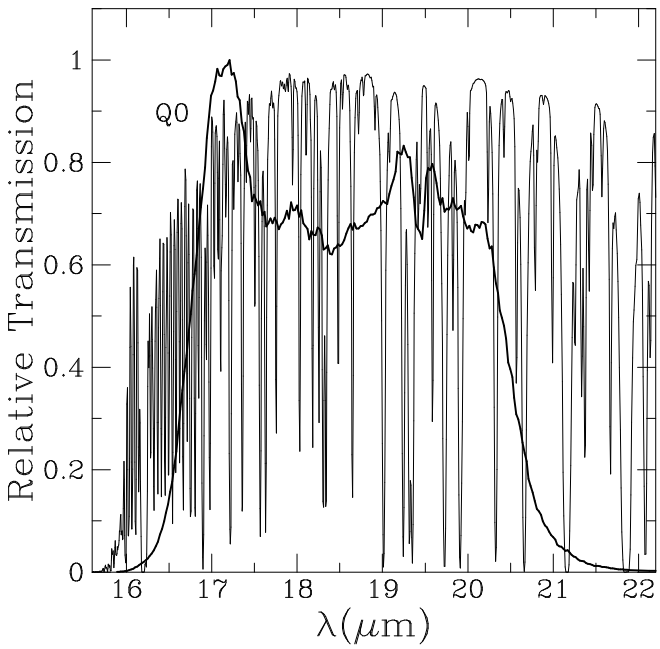

Fig. 4. Filter transmission times detector response at 20 μm, Q_0 (broad line) and the Earth's atmospheric transmission (thin line)

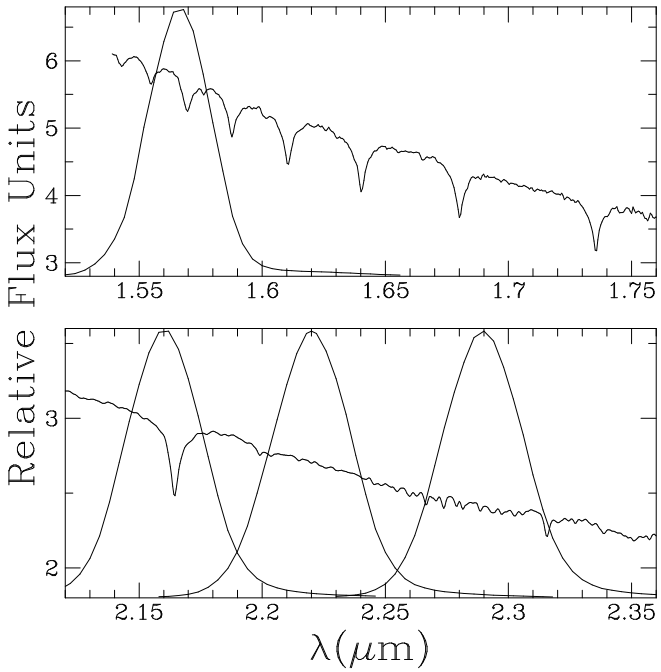

Fig. 5. Medium resolution H and K band spectra of HR 2421 (van der Bliek, in prep.) and the filter profiles of the narrow-band NIR filters

actually calculate the colours, we first have to define an absolute calibration at 10 and 20 μm.

The work by M95 does not cover the 10 and 20 μm bands. We therefore examine how her black body approximation compares with some of the most recent 10 and 20 μm calibrations: Rieke et al. (1985, hereafter RLL85) and Cohen et al. (1992, hereafter CWBD92). RLL85 and CWBD92 both present an absolute calibration of Vega (Table 2). The 10 μm calibration by RLL85 is based on direct measurements and their 20 μm calibration is an extrapolation of the 10 μm calibration. The calibration of Vega presented by CWBD92 is given by a synthetic spectrum, tied to the absolute calibration of Hayes (1985) at 5556 Å. To compare the results of CWBD92 with the calibration by M95, we scale the Vega fluxes to the V flux found by M95: $F(5556\ \text{Å})=3.46\ 10^{-11}\ \text{Wm}^{-2}\text{nm}^{-1}$. We convert the Vega fluxes by RLL85 and CWBD92 into zero-magnitude fluxes under the assumption that Vega has $K{=}N{=}0.02$ and $Q{=}0.05$ (RLL85; IRAS Explanatory Supplement 1988). Table 2 lists the fluxes of Vega by RLL85 and CWBD92 as well as the zero-magnitude fluxes corresponding to these Vega fluxes. Figure 6 displays the RLL85 and CWBD92 zero-magnitude fluxes relative to the extrapolation of the M95 calibration and we find that the M95 calibration approximates these calibrations within 5%. This is within the uncertainties of the absolute calibrations of RLL85 and CWBD92. We have therefore also adopted the M95 calibration for 10 and 20 μm photometry (Table 1).

Based on this MIR calibration we have calculated the colours of the Sun (Table 3) from the solar spectrum by Labs & Neckel (1970). The solar V magnitude was calibrated with the Vega spectrum by Dreiling & Bell (1980) under the assumption that $V_{\rm Vega}$=+0.03. In Table 3 the *calculated magnitudes* of β Hyi and of α CenA are also given. The V magnitudes are from Rufener (1988).

Table 2. The absolute fluxes of Vega by Rieke et al. (1985, RLL85) and Cohen et al. (1992, CWBD92) and the zero-magnitude fluxes corresponding to these Vega fluxes. The uncertainties of these calibrations are about 3% at 10 μm and 5% at 20 μm

filter	λ (μm)	F_λ(Vega) (W m^{-2} nm^{-1})	$F_\lambda(m_\lambda = 0)$ (W m^{-2} nm^{-1})
Rieke et al. 1985			
	10	1.21 10^{-15}	1.24 10^{-15}
	20	7.79 10^{-17}	8.16 10^{-17}
Cohen et al. 1992			
8.7	8.756	1.97 10^{-15}	2.00 10^{-15}
N	10.472	9.69 10^{-16}	9.87 10^{-16}
11.7	11.653	6.35 10^{-16}	6.46 10^{-16}
20	20.130	7.22 10^{-17}	7.56 10^{-17}

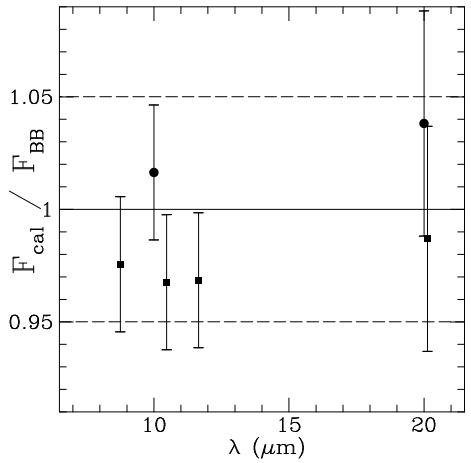

Fig. 6. Zero-magnitude fluxes by Rieke et al. (1985, RLL85) (circles) and Cohen et al. (1992, CWBD92) (squares) relative to the black body calibration by Mégessier (1995)

4. The observational data base

Data from the complete IR photometric data archive at La Silla have been used, extending the data base of BMS91 to July 1994 by 5 years. The observations were made at the ESO 1 m, 2.2 m or 3.6 m telescopes with single channel photometers and detector-filter combinations as described in Sect. 2. The systems are quite homogeneous, due to the fact that the detectors and filters of the three systems are identical. In addition, each telescope had in principle its own infrared instrumental system.

Table 3. The colours of the Sun and the *calculated magnitudes* of β Hyi (HR 0098) and α CenA (HR 5459)

filter	λ (μm)	Solar colours ($V-[\lambda]$)	β Hyi Magnitudes	α CenA Magnitudes
V	0.5556		2.82	-0.03
N	11.055	1.56	1.26	-1.59
N_1	8.361	1.58	1.24	-1.61
N_2	9.787	1.57	1.25	-1.60
N_3	12.819	1.54	1.28	-1.57
Q_0	18.666	1.51	1.31	-1.54

We rejected all measurements with an airmass (X) larger than 1.7, because they are a source of potential difficulties (e.g. Manfroid & Heck 1983). When observing at large zenith distances, the airmass varies rapidly with time, and then its mean value during an observation is not well defined and in general all atmospheric disturbances increase significantly at high airmasses.

We extracted those nights that fulfilled the criteria laid out in Table 4. A new night was defined whenever there was a gap between successive observations larger than 3.6 and 6.5 hours for the NIR and MIR observations, respectively. We only kept nights in which more than 17 (NIR) or 8 (MIR) stars were observed. We also required the nights to have more than 15 (NIR) or 5 (MIR) measurements with an airmass smaller than 1.1 and more than 10 (NIR) or 8 (MIR) measurements with an airmass larger than 1.35. These criteria minimize drifts, by splitting long nights into parts and keeping only those nights for which the reduction parameters can be calculated fairly accurately, so these parameters can be checked for anomalies. Bad nights were edited or deleted. We ended up with 213 nights with NIR and 36 nights with MIR photometry which fulfilled all these criteria.

The constraints used for the NIR are much stronger than the constraints used by BMS91, the reason being that we had many more nights to work with than BMS91. The constraints for the MIR observations are less severe than for the NIR observations, because these measurements are more time consuming, and therefore fewer stars were measured per night. The *broad*-band and *narrow*-band NIR data were reduced as one dataset.

5. The reduction method

As pointed out in Sects. 2 and 4, the different systems used are quite homogeneous and atmospheric variations

Table 4. Constraints on the nights and the number of useful nights. All measures with an airmass $X > 1.7$ were rejected

	NIR	MIR
gap (in hours)	< 3.6	< 6.5
min. # of stars	17	8
min. # of measures with $X < 1.1$	15	5
min. # of measures with $X > 1.35$	10	4
# of useful nights	213	36

produce only small shifts in effective wavelengths. Observations made on different nights or at different telescopes differ in zeropoints only. This allows us to use a global reduction method in which all observations of all nights and telescopes can be reduced at once. Such a method, called a 'multi night - multi instrument' method combines all observations in one computation, in which zeropoints and extinction coefficients are solved for each night (cf. Sterken & Manfroid 1992). For each star the magnitude outside the atmosphere, $m_{\rm out}$, is

$$m_{\rm out} = m - kX + z, \quad (3)$$

where m is the instrumental magnitude, k the extinction coëfficient, X the airmass and z the zeropoint. When combining the observations of several nights and several instruments one has to minimize the following function:

$$\phi(k_{n,f}, m_{{\rm out},c,f}, z_{n,f}) = \sum_n \sum_i \sum_c \sum_f (m_{c,f,i} - k_{n,f}X_i + z_{n,f} - m_{{\rm out},c,f})^2, \quad (4)$$

where the subscript n indicates the night, f the filter, c the constant star and i the measurement. Manfroid (1993) presents a reduction algorithm based on this principle that is implemented in the RANBO2 reduction package (Manfroid & Bouchet 1994), which we used for the reduction of the data.

An important feature of this method is that both calibration stars with known values in the natural system as well as new stars with unknown values, but constant in flux, are used. The first are the standard stars, the second are the constant stars. Using measurements of any constant star, even with unknown values, increases the number of useful stars considerably and it is this feature that makes this method more powerful than others for defining a set of standard stars. In principle only the values of one star need to be known, which is exactly what we used for defining the set of standards in the ESO IR system (Sect. 3).

An additional advantage of the algorithm used in the RANBO2 package is that instead of determining extinction coefficients either from a least squares fit through many observations of the same star at different airmasses, the so called Bouguer lines, or from values of standard stars, all measurements of all calibration stars are used. Furthermore it is possible to impose constraints between extinction coefficient variations in different bands, as well as between zeropoint variations. In general, a scheme as used in the RANBO2 reduction package is less dependent on the validity of the standard scale used, than a method only using stars with standard values (e.g. Harris et al. 1981; Popper 1982) and is more flexible than a method relying on Bouguer lines only.

6. The photometry of the standard stars

In the final stage of the data reduction we used as calibration stars all 'constant' stars: stars that were apparently stable and well-observed. These stars were found by running the program several times (see also Manfroid & Heck 1983) and editing the raw data between each iteration. As the reduction proceeded, some other stars proved to be valuable standard stars and were included.

The calibration stars and their data are presented in Tables 5-7. Table 5 contains the broadband NIR photometry, Table 6 the narrowband NIR photometry and Table 7 the MIR photometry. For each filter the magnitude, standard deviation and number of measurements are listed. We only list the magnitude in a band if there are 3 or more measurements available in that band. Tables 5-7 are not printed in this paper, but can easily be retrieved from the Centre de Données de Strasbourg (CDS) via email following the instructions published in the editorial notices of Astronomy and Astrophysics (January edition).

6.1. *The NIR photometry*

We selected the NIR calibration stars from the archive data with as starting point the standard star list of BMS91. We extended their list not only in number of stars but also to fainter stars, down to $K \simeq 9$. This is to a large extent the result of the observations performed in the framework of the Key Programme No. 7-00847K, 'Infrared Standard Stars for ISO'. The purpose of this Key Programme was to compile a set of southern stars to serve as photometric standards for the Infrared Space Observatory ISO (cf. van der Bliek et al. 1992). Using the list by BMS91 as a basis, a list of candidate standard stars was compiled applying the following criteria. The stars should be non-variable and single. The whole set of stars should be distributed as uniformly as possible over spectral type and magnitude and should have a homogeneous distribution over the sky. On the basis of IRAS data an estimate of a possible IR excess was made for each star. Stars which show a clear IR excess at 25 and 60 μm were omitted. Stars were selected from the IR standard star lists of the South African Astronomical Observatory SAAO (Carter 1990), the Anglo-Australian Observatory AAO (Allen & Cragg 1983) and the Cerro Tololo Inter-American

Observatory CTIO (Elias et al. 1983). The sample is extended with a selection of stars from the Bright Star Catalogue (Hoffleit 1982) and the Henry Draper Catalogue (1918) and we used these two catalogues as well as the SIMBAD data base and the Hipparcos Input Catalogue to discard multiple and variable stars. In the final analysis we also rejected stars with peculiar NIR colours.

We compared the ESO NIR broadband photometry with the NIR photometry of the AAO, CTIO, SAAO and MSSSO (Fig. 7). In Fig. 7 linear fits are shown, representing the colour transformations from the ESO photometric system to the other systems. We used a regression procedure, which took into account the errors in both coordinates as described in Numerical Recipes Sect. 15.3 (Press et al. 1992). We also derived the transformations from the other systems to the ESO system. The results are given in Table 8, where a, b, c and d are defined as follows:

$$M_{\rm other} - M_{\rm ESO} = a + b \times (J_{\rm ESO} - K_{\rm ESO}) \qquad (5)$$

and

$$M_{\rm ESO} - M_{\rm other} = c + d \times (J_{\rm other} - K_{\rm other}) \qquad (6)$$

As can be seen in Fig. 7, there is hardly any colour dependence in the transformation of any of the ESO photometric bands to other systems, except for the AAO L', CTIO J and L' and MSSSO J and L' which show a slight colour dependence. The colour dependence of the CTIO J band was also found by BMS91. These authors noticed that the effect does not depend on source brightness. The present data confirm their result, also for the colour dependence of the L' band. We note however that the fits are poor, and that the colour dependencies are systematically less when there are more overlapping stars. We find small offsets in the zeropoints of the magnitude scales. The offsets with respect to the AAO and MSSSO photometry are less than 0.01 mag., except for the MSSSO J band (0.02 mag.). With respect to the CTIO and SAAO the ESO zeropoints are offsetted by about 0.02 mag., except for the CTIO L' band (0.04 mag.).

We find that the broadband photometry has accuracies of the order of 0.02 mag. in J, H, K and L' and 0.03 mag. in M (see Table 5). The narrowband photometry has accuracies of the order of 0.02 mag. in H_0, $Br\gamma$, K_0 and CO and 0.03 mag. in L_0 (Table 6).

6.2. *The MIR photometry*

In Fig. 8 we compare our MIR photometry with the data of Thomas et al. (1973) at 8.4, 10.2 and 11.2 μm. There are 18 stars in common. The differences in magnitudes between N_1 and [8.4] and N_2 and [10.2] are large, about

Table 8. The colour transformations from ESO NIR photometry to AAO, CTIO, SAAO and MSSSO NIR photometry: $M_{\rm other} - M_{\rm ESO} = a + b \times (J_{\rm ESO} - K_{\rm ESO})$ and vice versa: $M_{\rm ESO} - M_{\rm other} = c + d \times (J_{\rm other} - K_{\rm other})$. n is the number of overlapping stars

$M_{\rm other} - M_{\rm ESO} = a + b \times (J_{\rm ESO} - K_{\rm ESO})$					
	n	a	σ_a	b	σ_b
AAO					
J	42	-.008	.004	-.004	.013
H	42	.009	.004	.001	.011
K	42	-.008	.004	.005	.011
L'	21	-.011	.004	-.045	.014
CTIO					
J	20	-.018	.003	-.105	.011
H	20	-.006	.002	-.039	.007
K	20	-.017	.002	-.009	.008
L'	16	-.037	.004	.033	.012
SAAO					
J	115	-.021	.002	.003	.004
H	115	-.015	.002	-.024	.004
K	115	-.020	.002	-.003	.004
L'	88	-.029	.008	.016	.000
MSSSO					
J	26	-.021	.003	-.052	.012
H	26	-.002	.003	-.018	.009
K	26	-.006	.003	-.008	.009
L'	26	-.002	.002	.016	.010
$M_{\rm ESO} - M_{\rm other} = c + d \times (J_{\rm other} - K_{\rm other})$					
	n	c	σ_c	d	σ_d
AAO					
J	42	.009	.004	-.001	.013
H	42	-.009	.004	-.000	.011
K	42	.008	.004	-.005	.011
L'	42	.011	.004	.043	.014
CTIO					
J	20	.018	.003	.111	.012
H	20	.006	.002	.042	.008
K	20	.017	.003	.009	.009
L'	16	.037	.004	-.037	.013
SAAO					
J	115	.022	.002	-.005	.004
H	115	.015	.002	.023	.004
K	115	.020	.002	.002	.004
L'	88	.029	.007	-.016	.000
MSSSO					
J	26	.023	.003	.051	.012
H	26	.003	.003	.018	.010
K	26	.006	.003	.008	.009
L'	26	.002	.002	-.018	.010

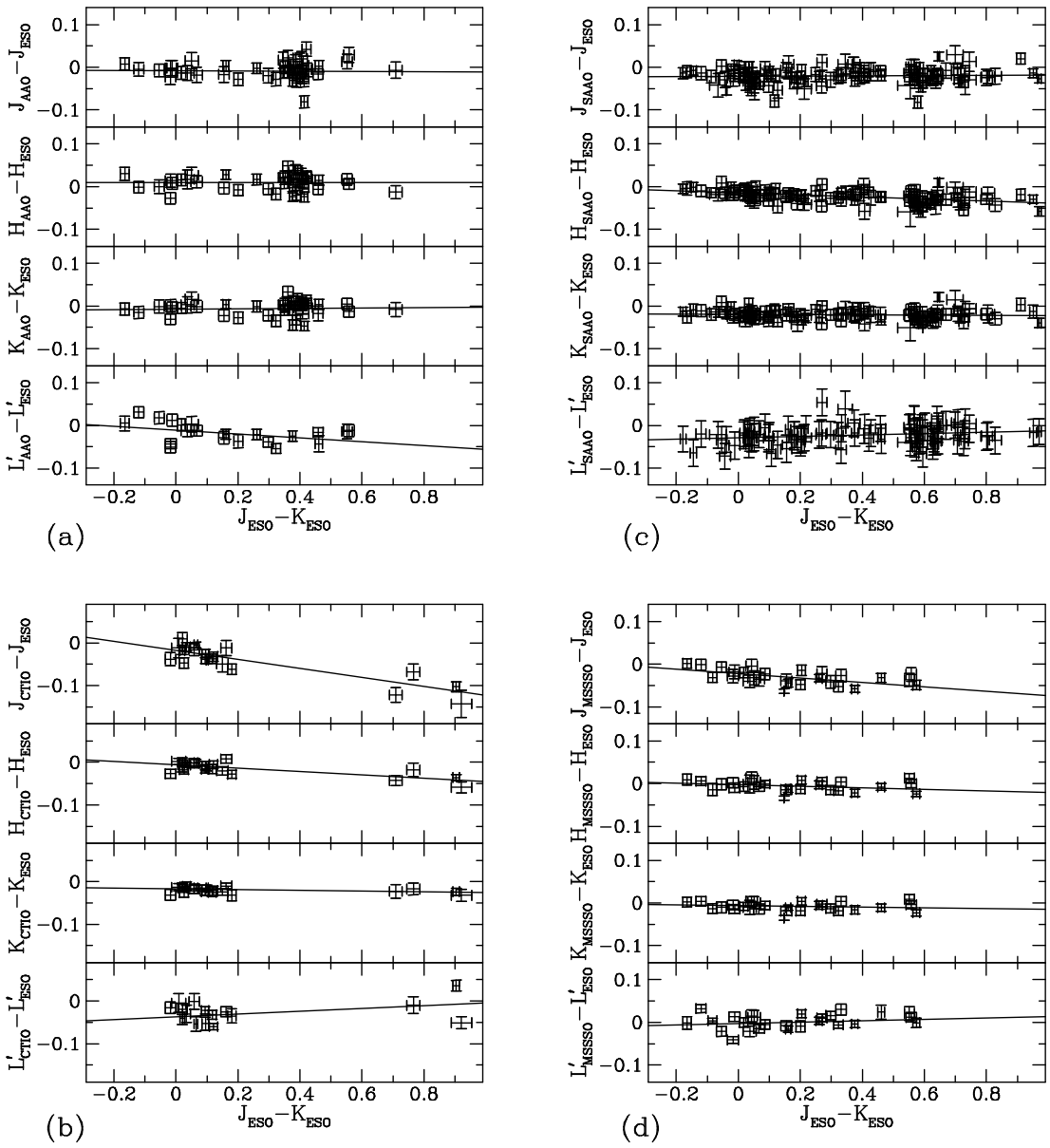

Fig. 7. Comparing the ESO NIR photometry with **a)** the AAO photometry, **b)** the CTIO photometry, **c)** the SAAO photometry and **d)** the MSSSO photometry

0.1 mag., but there is no clear correlation between magnitude difference and colour. The apparent colour dependence between N_3 and [11.2] maybe attributed to the difference in effective wavelength: 12.8 μm for N_3, instead of $\sim$11 μm. The same holds true for the correlation between the magnitude differences and the stellar brightness (Fig. 9). A meaningful comparison could not be made with Simon et al. (1972), Tokunaga et al. (1984) and RLL85, as there were only 1 or 2 stars in common.

The accuracy of the MIR photometry of the standard stars is about 0.03 mag. for the 10 μm and about 0.05 mag. for the 20 μm photometry. We note that the magnitude scale for the Q_0 photometry is tied to only one observation of one of the solar analogues, β Hyi (Table 7).

7. Concluding remarks

We have presented the ESO IR photometric system, which *was* available from 1983 to 1994. Although this particular system is not offered anymore, defining the system and presenting the photometric data is of importance for the calibration of present day and also future IR observations. NIR imaging and photometry with array detectors on medium-sized telescopes can go as deep as K magnitude 16 to 20 and the ESO faint standard stars are

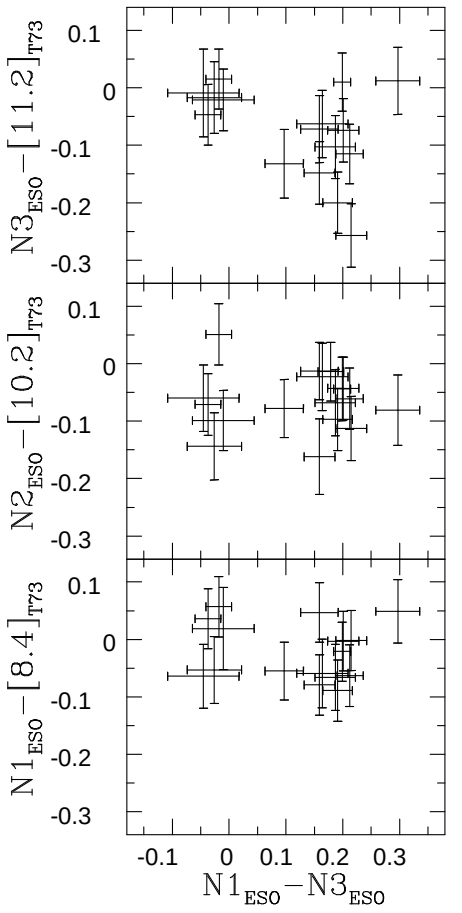

Fig. 8. The colour dependence of the differences between the 10 μm photometry of ESO and of Thomas et al. (1973) at 8.4, 10.2 and 11.2 μm. Note that the effective wavelengths of the ESO filters are N_1: 8.3 μm, N_2: 9.7 μm, N_3: 12.8 μm

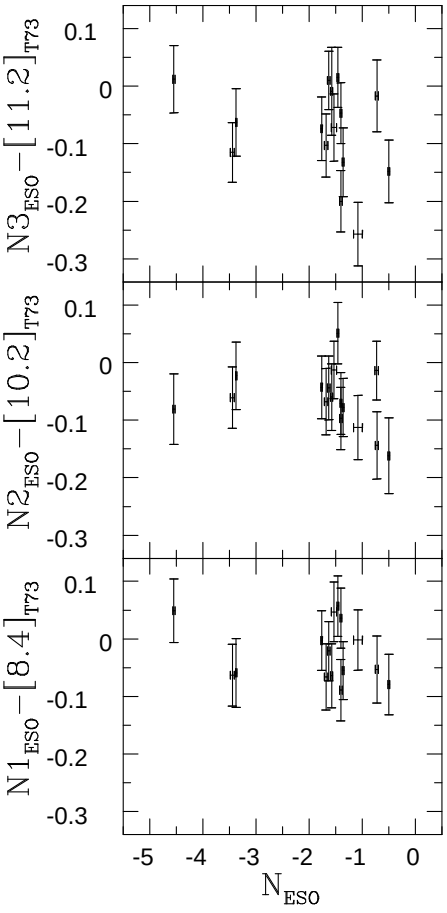

Fig. 9. The brightness dependence of the differences between the 10 μm photometry of ESO and of Thomas et al. (1973) at 8.4, 10.2 and 11.2 μm. Note that the effective wavelengths of the ESO filters are N_1: 8.3 μm, N_2: 9.7 μm, N_3: 12.8 μm

essential for the calibration of these data. Likewise, the MIR standard stars are being used for the calibration of the data of the current 10 μm arrays. In addition to ground-based applications, these photometric data are also being used for the calibration of ISO observations. For a number of stars, predictions of the far IR (FIR) fluxes will be made on the basis of synthetic stellar spectra which will be tied to NIR photometric data (e.g. van der Bliek et al. 1992).

In a programme like the ISO calibration programme data of various photometric systems are used and the photometric data is converted into absolute fluxes. Using data of more than one photometric system can give rise to systematic errors due to differences in the definition of the zeropoints. More generally, errors in absolute fluxes derived from the IR photometry arise from the uncertainty in the absolute calibration and from the combination of the choice of the zeropoints and the absolute calibration adopted. The uncertainty in the absolute calibration is about 2% in the NIR and 5% in the MIR. Matching the zeropoints of the magnitude scale to the absolute calibration introduces an uncertainty of about 2% in the NIR and 5% in the MIR. Taking into account also the mean errors in the photometric data, 0.02 mag. in the NIR and 0.03 mag. at 10 μm, we conclude that the derived absolute fluxes have an uncertainty of about 4% for the NIR and 6% for the 10 μm photometry.

Acknowledgements. We thank all IR photometrists at La Silla are thanked for their contribution, with special thanks to P. Hammersley, T.L. Lim, L. Metcalfe, M. de Muizon and A. Salama, who participated in the observations for the ESO Key Programme 'Infrared Standards for ISO'. We thank the PI of this Key Programme, H.J. Habing, for initialising and supporting the programme, because it stimulated putting together all there was available on ESO IR photometry. H.J. Habing and J. Koornneef provided constructive comments, which improved the paper enormously. This research also made use of ESO Test & Reserved time. We thank the ESO IR team for their technical support, with special thanks to J. Roucher for measuring the transmission curves and to R. Vega, who participated

in most of the observations. This research made use of the SIMBAD database, operated at the CDS, Strasbourg, France and of the Hipparcos Input Catalogue.

References

Allen D.A., Cragg T.A., 1983, MNRAS 203, 777
Aspin C., 1995, (priv. communication)
Bersanelli M., Bouchet P., Falomo R., 1991, A&A 252, 854
Blackwell D.E., Petford A.D., Shallis M.J., 1980, A&A 82, 249
Bouchet P., 1989, IR photometers, ESO Manual No. 11
Bouchet P., Manfroid J., Schmider F.-X., 1991, A&AS 91, 409 (BMS91)
Carter B.S., 1990, MNRAS 242, 1
Cohen M., Walker R.G., Barlow M.J., Deacon J.R., 1992, AJ 104, 1650 (CWBD92)
Henry Draper Catalogue, Harvard Annals, 93-99, 1918-1924
Dreiling L.A., Bell R.A., 1980, ApJ 241, 736
Elias J.H., Frogel J.A., Matthews K., Neugebauer G., 1982, AJ 87, 1029
Elias J.H., Frogel J.A., Hyland A.R., Jones T.J., 1983, AJ 88, 1027
Hardorp J., 1978, A&A 63, 383
Hardorp J., 1982, A&A 105, 120
Harris W.E., Fitzgerald M.P., Reed B.C., 1981, PASP 93, 507
Hayes D.S., 1985, In: Calibration of Fundamental Stellar Quantities. In: Hayes D.S. et al. (eds.), p. 225
Hoffleit D., 1982, The Bright Star Catalogue (fourth revised edition), Yale University Observatory, New Haven
IRAS Explanatory Supplement 1988, in: Beichmann C. et al. (eds.)
Johnson H.L., 1965, Comm. Lun. Plan. Lab. 3, 73
Jones T.J., Hyland A.R., 1982, MNRAS 200, 509
King I., 1952, AJ 57, 253
Labs D., Neckel H., 1970, Solar Phys. 15, 79
Manduca A., Bell R.A., 1979, PASP 91, 848
Manfroid J., Heck A., 1983, A&A 120, 302
Manfroid J., 1993, A&A 271, 714
Manfroid J., Bouchet P., 1994, Manual for RANBO2, a package for photometric reductions, ESO, Santiago
McGregor P.J., 1994, PASP 106, 508
Mégessier C., 1995, A&A 296, 771 (M95)
Press W.H. et al., 1992, Numerical Recipes in Fortran: the art of scientific computing. Cambridge University Press, Cambridge
Popper D.M., 1982, PASP 94, 204
Rieke G.H., Lebofsky M.J., Low F.J., 1985, AJ 90, 900 (RLL85)
Rufener F., Nicolet B., 1988, A&A 206, 357
Rufener F., 1988, Catalogue of stars measured in the Geneva Observatory Photometric System (fourth edition), Observatoire de Genèva, Sauverny
Simon T., Morrison D., Cruikshank D.P., 1972, ApJ 177, L17
Sterken C., Manfroid J., 1992, Astronomical Photometry. A Guide. Kluwer Academic Publishers, Dordrecht
Thomas J.A., Hyland A.R., Robinson G., 1973, MNRAS 165, 201
Tokunaga A.T., 1984, AJ 89, 172
van der Bliek N.S., et al., 1992, The Messenger 70, 28
van der Bliek N.S., 1996, (in preparation)
Young A.T., Milone E.F., Stagg C.R., 1993, In: 'Stellar Photometry - Current Techniques and Future Developments', IAU Coll. 136. In: Butler C.J. and Elliott I. (eds.), p. 235
Young A.T., Milone E.F., Stagg C.R., 1994, A&AS 105, 259